Journal of Marine Science and Technology

Volume 24 | Issue 4 Article 9

SHAPE OPTIMIZATION OF TWO-CHAMBER MUFFLERS HYBRIDIZED WITH MULTIPLE PARALLEL DISSIPATIVE TUBES USING SIMULATED ANNEALING METHOD

Ho-Chih Cheng
Department of Mechanical and Automation Engineering, Chung Chou University of Science and Technology, Taiwan, R.O.C.

Min-Chie Chiu
Department of Mechanical and Automation Engineering, Chung Chou Uni-versity of Science and Technology, Taiwan, R.O.C., minchie.chiu@msa.hinet.net

Recommended Citation

Cheng, Ho-Chih and Chiu, Min-Chie (2016) "SHAPE OPTIMIZATION OF TWO-CHAMBER MUFFLERS HYBRIDIZED WITH MULTIPLE PARALLEL DISSIPATIVE TUBES USING SIMULATED ANNEALING METHOD," *Journal of Marine Science and Technology*: Vol. 24: Iss. 4, Article 9.
DOI: 10.6119/JMST-016-0303-1
Available at: https://jmstt.ntou.edu.tw/journal/vol24/iss4/9

Journal of Marine Science and Technology, Vol. 24, No. 4, pp. 744-758 (2016)
DOI: 10.6119/JMST-016-0303-1

SHAPE OPTIMIZATION OF TWO-CHAMBER MUFFLERS HYBRIDIZED WITH MULTIPLE PARALLEL DISSIPATIVE TUBES USING SIMULATED ANNEALING METHOD

Ho-Chih Cheng and Min-Chie Chiu

Key words: multiple parallel dissipative tube, two-chamber, resonating, simulated annealing.

ABSTRACT

Mufflers hybridized with a single dissipative tube have been extensively researched; however, there has been a palpable lack of work directed toward mufflers conjugated with multiple parallel dissipative tubes that disperse venting fluid and reduce secondary noise. That being so, an analysis of the Sound Transmission Loss (*STL*) of two-chamber mufflers with multiple parallel dissipative tubes that are optimally designed to perform within a limited space will be considered, here.

By using a decoupled numerical method, a four-pole system matrix for evaluating acoustic performance (*STL*) emerges. During the optimization process, a simulated annealing (*SA*) method, which is a robust scheme utilized to search for the global optimum by imitating a physical annealing process, is used. Before dealing with a broadband noise, the *STL*'s maximization relative to a one-tone noise (400 Hz) is offered to confirm the *SA* method's reliability. Subsequently, the mathematical model is checked for accuracy, and three types of mufflers (mufflers A-C) hybridized with one, two, and four parallel dissipative tubes are assessed.

To bring into focus the acoustical interaction between the dissipative tube (with wool filled within a set of perforated tubes) and the non-dissipative tube (without wool within the perforated tubes), two types of mufflers (one and four non-dissipative tubes) have been surveyed. Results divulge that the maximal *STL* is located at the desired tone, and the acoustical performance of two-chamber mufflers conjugated with multi-dissipative tubes decreases as a result of the decrement of the acoustical function for acoustical elements (II) and (III).

Consequently, optimally designed two-chamber mufflers with multiple parallel dissipative tubes that avoid secondary noise induced by high speed flow while simultaneously maximizing acoustical performance within a constrained space are preferable.

I. INTRODUCTION

Morse (1939) began research on mufflers that reduced high frequency noise using a dissipative duct (a duct lined with sound absorbing material). In 1975, Ko (1975) assessed the sound transmission loss in acoustically lined flow ducts separated by porous splitters. Intent on increasing acoustical performance, the assessment of an internal perforated tube was introduced and discussed by Sullivan and Crocker (1978). Based on the coupled equations derived by Sullivan and Crocker, a series of theories and numerical techniques in decoupling the acoustical problems were proposed (Sullivan, 1979; Jayaraman and Yam, 1981; Thawani and Jayaraman, 1983; Munjal et al., 1987). Subsequently, Munjal (1987) and Peat (1988) published the generalized and numerical decoupling methods. Also, Cummings and Chang (1988) developed a modal method for analyzing a finite length dissipative flow duct silencer with internal mean flow in the absorbent. Peat (1991), addressing the volume modulus, used a transfer matrix for evaluating the acoustical performance of an absorption silencer element. Then, Sathyanarayana and Munjal (2000) developed a hybrid approach for the prediction of noise radiation emitted from an engine exhaust system.

Subsequently, using a one-dimensional analytical method and a three-dimensional boundary element method (BEM), Selamet et al. (2001, 2003) assessed the acoustical attenuation for perforated concentric absorbing silencers and hybrid silencers. Then, Xu et al. (2004) investigated sound attenuation in dissipative expansion chambers using the characteristic equation. Later, Kar and Munjal (2005) expanded the assessment on a muffler hybridized by multiply interacting perforated ducts using a generalized analysis. Sohei et al. (2006) developed a mathematic model for an elliptical muffler that was equipped with a perforated pipe within a higher-order mode in

Paper submitted 05/14/15; revised 11/03/15; accepted 03/03/16. *Author for correspondence: Min-Chie Chiu (e-mail: minchie.chiu@msa.hinet.net).*
Department of Mechanical and Automation Engineering, Chung Chou University of Science and Technology, Taiwan, R.O.C.

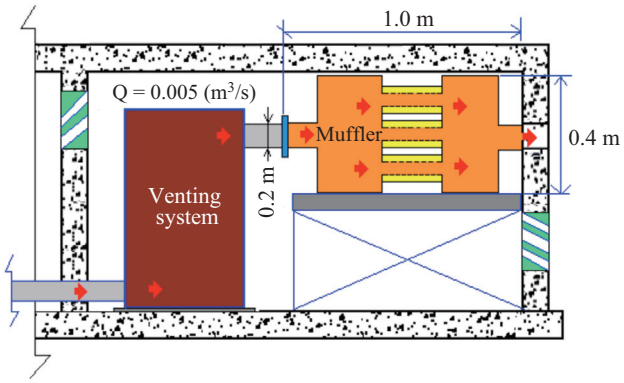

Fig. 1. Noise elimination on a venting system within a limited space.

a zero speed flowing field. Consequently, Lee and Selamet (2006) widened the BEM (Boundary Element Method) numerical assessment on a resonator with or without a fiber filled inner cavity. The above studies have provided various solutions for solving the complicated acoustical field problem for perforated mufflers. However, an assessment of a muffler's optimal design within a limited space was seldom addressed. Therefore, Chiu (2011a, 2011b, 2012) has examined the shaped optimization of a hybrid muffler hybridized with one dissipative tube within a constrained space.

Because research on mufflers conjugated with multiple parallel dissipative tubes that disperse venting fluid and reduce secondary noise has been overlooked, an analysis of the Sound Transmission Loss (*STL*) of two-chamber mufflers with multiple parallel dissipative tubes optimally designed to perform within a limited space is introduced.

Three types of two-chamber mufflers linked with multiple dissipative tubes (muffler A: a two-chamber muffler with one dissipative tube; muffler B: a two-chamber muffler with two dissipative tubes; muffler C: a two-chamber muffler with four dissipative tubes) are presented. It should also be noted that numerical decoupling methods used to form a four-pole system matrix are compatible with the simulated annealing method.

III. THEORETICAL BACKGROUND

Three types of two-chamber mufflers connected with multiple parallel dissipative tubes have been adopted for noise elimination in the venting system shown in Fig. 1. Before the acoustical fields of the mufflers were analyzed, the acoustical elements had been identified. As shown in Fig. 2, four types of muffler components, including four straight ducts, two sudden expanded ducts, two sudden contracted ducts, and multiple parallel dissipative ducts, are identified and marked as I, II, III, and IV. Additionally, the acoustical field within the muffler is represented by ten points. The outline dimension of the mufflers with multiple parallel dissipative ducts is shown in Fig. 3. As derived in previous works (Chiu, 2010a; Chiu, 2010b; Chiu, 2011a; Chiu, 2011b; Chiu and Chang, 2011; Chiu, 2012) and shown in appendices A-C, individual transfer matrices with respect to straight ducts, dissipative ducts, and sudden expanded/contracted ducts are described below.

1. Muffler A (A Two-Chamber Muffler Hybridized with One Dissipative Tube)

As indicated in Fig. 2, for the acoustical element (I), the four-pole matrix between nodes 1 and 2 is (Chiu, 2010a; Chiu, 2010b; Chiu, 2011a; Chiu, 2011b; Chiu and Chang, 2011; Chiu, 2012)

$$\begin{pmatrix} p_1 \\ \rho_o c_o u_1 \end{pmatrix} = f_1(L_i, D_i, M_i) \begin{bmatrix} TS1_{1,1} & TS1_{1,2} \\ TS1_{2,1} & TS1_{2,2} \end{bmatrix} \begin{pmatrix} p_2 \\ \rho_o c_o u_2 \end{pmatrix} \quad (1)$$

For the acoustical element (II), the four-pole matrix between nodes 2 and 3 is (Chiu, 2010a; Chiu, 2010b; Chiu, 2011a; Chiu, 2011b; Chiu and Chang, 2011; Chiu, 2012)

$$\begin{bmatrix} p_2 \\ \rho_o c_o u_2 \end{bmatrix} = \begin{bmatrix} TSE1_{1,1} & TSE1_{1,2} \\ TSE1_{2,1} & TSE1_{2,2} \end{bmatrix} \begin{bmatrix} p_3 \\ \rho_o c_o u_3 \end{bmatrix} \quad (2)$$

Similarly, the four-pole matrix between nodes 3 and 4 is

$$\begin{pmatrix} p_3 \\ \rho_o c_o u_3 \end{pmatrix} = f_2(L_i, D_i, M_i) \begin{bmatrix} TS2_{1,1} & TS2_{1,2} \\ TS2_{2,1} & TS2_{2,2} \end{bmatrix} \begin{pmatrix} p_4 \\ \rho_o c_o u_4 \end{pmatrix} \quad (3)$$

For the acoustical element (III), the four-pole matrix between nodes 4 and 5 is (Chiu, 2010a; Chiu, 2010b; Chiu, 2011a; Chiu, 2011b; Chiu and Chang, 2011; Chiu, 2012)

$$\begin{bmatrix} p_4 \\ \rho_o c_o u_4 \end{bmatrix} = \begin{bmatrix} TSC1_{1,1} & TSC1_{1,2} \\ TSC1_{2,1} & TSC1_{2,2} \end{bmatrix} \begin{bmatrix} p_5 \\ \rho_o c_o u_5 \end{bmatrix} \quad (4)$$

As shown in previous works (Chiu, 2010a; Chiu, 2010b; Chiu, 2011a; Chiu, 2011b; Chiu and Chang, 2011; Chiu, 2012) and derivation in Appendix A, for an acoustical element (IV), the four-pole matrix between nodes 5 and 6 yields

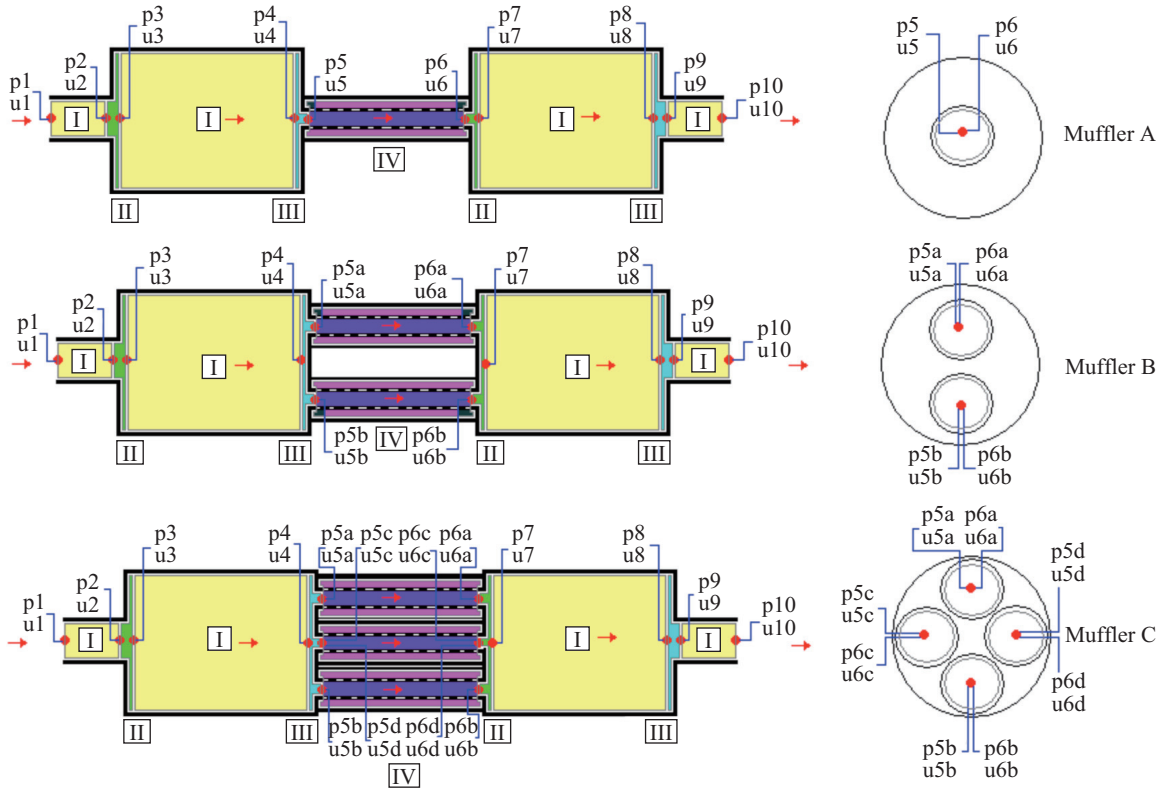

Fig. 2. Acoustical elements in three types of two-chamber mufflers hybridized with dissipative tubes (muffler A-muffler C).

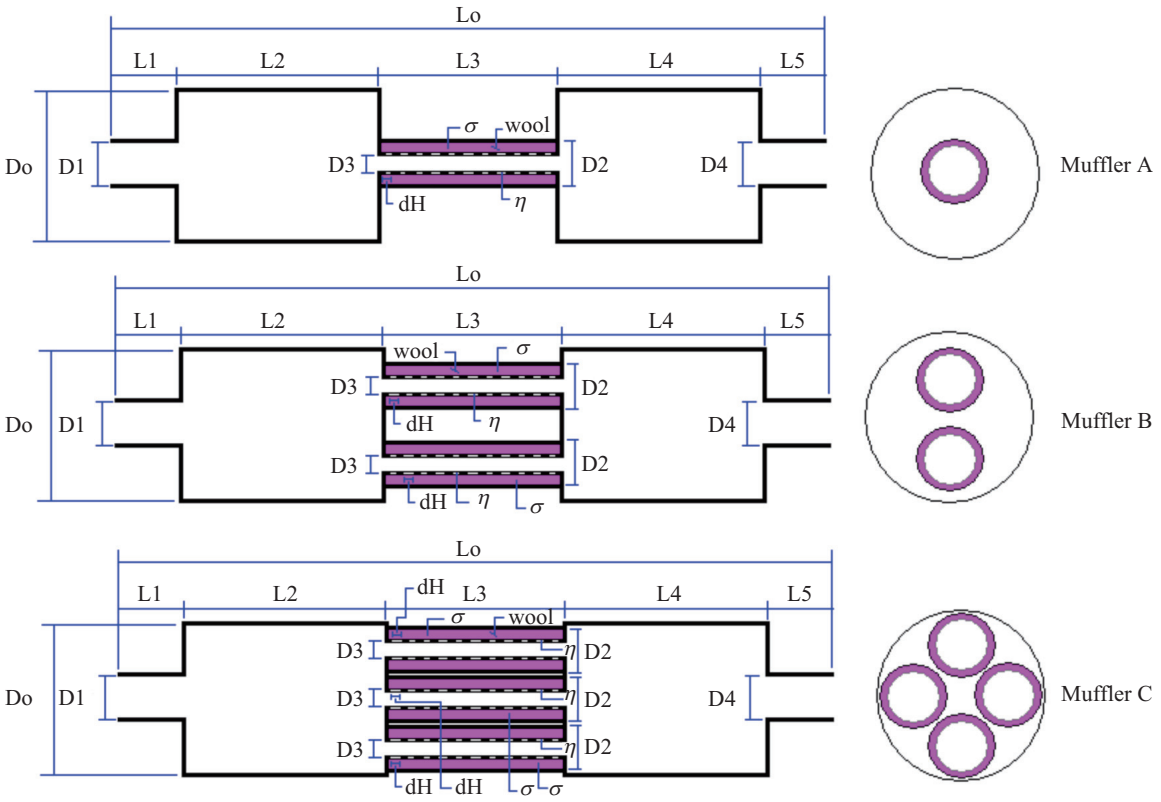

Fig. 3. The outline dimension of three kinds of two-chamber mufflers hybridized with dissipative tubes (muffler A-muffler C).

$$\begin{bmatrix} p_5 \\ \rho_o c_o u_5 \end{bmatrix} = \begin{bmatrix} TPW1_{1,1} & TPW1_{1,2} \\ TPW1_{2,1} & TPW1_{2,2} \end{bmatrix} \begin{bmatrix} p_6 \\ \rho_o c_o u_6 \end{bmatrix} \tag{5}$$

Likewise, the four-pole matrix between nodes 6 and 7 for a sudden expanded duct is

$$\begin{bmatrix} p_6 \\ \rho_o c_o u_6 \end{bmatrix} = \begin{bmatrix} TSE2_{1,1} & TSE2_{1,2} \\ TSE2_{2,1} & TSE2_{2,2} \end{bmatrix} \begin{bmatrix} p_7 \\ \rho_o c_o u_7 \end{bmatrix} \tag{6}$$

The four-pole matrix between nodes 7 and 8 in a straight duct is

$$\begin{pmatrix} p_7 \\ \rho_o c_o u_7 \end{pmatrix} = f_3(L_i, D_i, M_i) \begin{bmatrix} TS3_{1,1} & TS3_{1,2} \\ TS3_{2,1} & TS3_{2,2} \end{bmatrix} \begin{pmatrix} p_8 \\ \rho_o c_o u_8 \end{pmatrix} \tag{7}$$

The four-pole matrix between nodes 8 and 9 for a sudden contracted duct is

$$\begin{bmatrix} p_8 \\ \rho_o c_o u_8 \end{bmatrix} = \begin{bmatrix} TSC2_{1,1} & TSC2_{1,2} \\ TSC2_{2,1} & TSC2_{2,2} \end{bmatrix} \begin{bmatrix} p_9 \\ \rho_o c_o u_9 \end{bmatrix} \tag{8}$$

Moreover, the four-pole matrix between nodes 9 and 10 in a straight duct is

$$\begin{pmatrix} p_9 \\ \rho_o c_o u_9 \end{pmatrix} = f_4(L_i, D_i, M_i) \begin{bmatrix} TS4_{1,1} & TS4_{1,2} \\ TS4_{2,1} & TS4_{2,2} \end{bmatrix} \begin{pmatrix} p_{10} \\ \rho_o c_o u_{10} \end{pmatrix} \tag{9}$$

The total transfer matrix assembled by multiplication is

$$\begin{pmatrix} p_1 \\ \rho_o c_o u_1 \end{pmatrix} = f_1(L_i, D_i, M_i) f_2(L_i, D_i, M_i) f_3(L_i, D_i, M_i) f_4(L_i, D_i, M_i) f_5(L_i, D_i, M_i)$$
$$\begin{bmatrix} TS1_{1,1} & TS1_{1,2} \\ TS1_{2,1} & TS1_{2,2} \end{bmatrix} \begin{bmatrix} TSE1_{1,1} & TSE1_{1,2} \\ TSE1_{2,1} & TSE1_{2,2} \end{bmatrix} \begin{bmatrix} TS2_{1,1} & TS2_{1,2} \\ TS2_{2,1} & TS2_{2,2} \end{bmatrix} \begin{bmatrix} TSC1_{1,1} & TSC1_{1,2} \\ TSC1_{2,1} & TSC1_{2,2} \end{bmatrix}$$
$$\begin{bmatrix} TPW1_{1,1} & TPW1_{1,2} \\ TPW1_{2,1} & TPW1_{2,2} \end{bmatrix} \begin{bmatrix} TSE2_{1,1} & TSE2_{1,2} \\ TSE2_{2,1} & TSE2_{2,2} \end{bmatrix} \begin{bmatrix} TS3_{1,1} & TS3_{1,2} \\ TS3_{2,1} & TS3_{2,2} \end{bmatrix} \begin{bmatrix} TSC2_{1,1} & TSC2_{1,2} \\ TSC2_{2,1} & TSC2_{2,2} \end{bmatrix}$$
$$\begin{bmatrix} TS4_{1,1} & TS4_{1,2} \\ TS4_{2,1} & TS4_{2,2} \end{bmatrix} \begin{pmatrix} p_{10} \\ \rho_o c_o u_{10} \end{pmatrix} \tag{10}$$

A simplified form is expressed in a matrix as

$$\begin{pmatrix} p_1 \\ \rho_o c_o u_1 \end{pmatrix} = \begin{bmatrix} T_{11}^* & T_{12}^* \\ T_{21}^* & T_{22}^* \end{bmatrix} \begin{pmatrix} p_{10} \\ \rho_o c_o u_{10} \end{pmatrix} \tag{11}$$

2. Muffler B (A Two-Chamber Muffler Hybridized with Two Dissipative Tubes)

Similarly, the acoustical four-pole matrix between nodes 1 and 2, nodes 2 and 3, nodes 3 and 4, nodes 7 and 8, nodes 8 and 9, and nodes 9 and 10 is the same as Eqs. (1)-(3) and Eqs. (7)-(9).

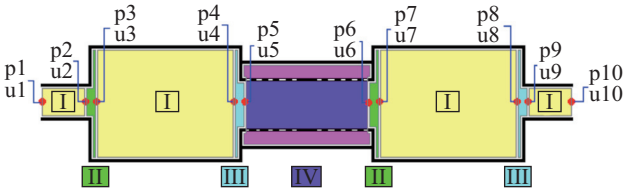

Fig. 4. Equivalent acoustical field for muffler hybridized with dissipative tubes (muffler B and muffler C).

As derived in Appendix B, for two parallel dissipative tubes connected to two chambers, the four-pole matrices between nodes 5a and 6a and nodes 5b and 6b can be combined into an equivalent matrix

$$\begin{bmatrix} p_5 \\ \rho_o c_o u_5 \end{bmatrix} = \begin{bmatrix} TPW1_{1,1} & \frac{1}{2} \cdot TPW1_{1,2} \\ 2 \cdot TPW1_{2,1} & TPW1_{2,2} \end{bmatrix} \begin{bmatrix} p_6 \\ \rho_o c_o u_6 \end{bmatrix} \tag{12}$$

where $[TPW1_{i,j}]$ is the four-pole matrix for a single dissipative tube.

The equivalent acoustical field of muffler B is shown in Fig. 4. Consequently, the total transfer matrix assembled by multiplication is

$$\begin{pmatrix} p_1 \\ \rho_o c_o u_1 \end{pmatrix} = f_1(L_i, D_i, M_i) f_2(L_i, D_i, M_i) f_3(L_i, D_i, M_i) f_4(L_i, D_i, M_i) f_5(L_i, D_i, M_i)$$
$$\begin{bmatrix} TS1_{1,1} & TS1_{1,2} \\ TS1_{2,1} & TS1_{2,2} \end{bmatrix} \begin{bmatrix} TSE1_{1,1} & TSE1_{1,2} \\ TSE1_{2,1} & TSE1_{2,2} \end{bmatrix} \begin{bmatrix} TS2_{1,1} & TS2_{1,2} \\ TS2_{2,1} & TS2_{2,2} \end{bmatrix} \begin{bmatrix} TSC1_{1,1} & TSC1_{1,2} \\ TSC1_{2,1} & TSC1_{2,2} \end{bmatrix}$$
$$\begin{bmatrix} TPW1_{1,1} & \frac{1}{2} \cdot TPW1_{1,2} \\ 2 \cdot TPW1_{2,1} & TPW1_{2,2} \end{bmatrix} \begin{bmatrix} TSE2_{1,1} & TSE2_{1,2} \\ TSE2_{2,1} & TSE2_{2,2} \end{bmatrix} \begin{bmatrix} TS3_{1,1} & TS3_{1,2} \\ TS3_{2,1} & TS3_{2,2} \end{bmatrix} \begin{bmatrix} TSC2_{1,1} & TSC2_{1,2} \\ TSC2_{2,1} & TSC2_{2,2} \end{bmatrix}$$
$$\begin{bmatrix} TS4_{1,1} & TS4_{1,2} \\ TS4_{2,1} & TS4_{2,2} \end{bmatrix} \begin{pmatrix} p_{10} \\ \rho_o c_o u_{10} \end{pmatrix} \tag{13}$$

A simplified form is expressed in a matrix as

$$\begin{pmatrix} p_1 \\ \rho_o c_o u_1 \end{pmatrix} = \begin{bmatrix} T_{11}^{**} & T_{12}^{**} \\ T_{21}^{**} & T_{22}^{**} \end{bmatrix} \begin{pmatrix} p_{10} \\ \rho_o c_o u_{10} \end{pmatrix} \tag{14}$$

3. Muffler C (A Two-Chamber Muffler Hybridized with Four Dissipative Tubes)

The acoustical four-pole matrix between nodes 1 and 2, nodes 2 and 3, nodes 3 and 4, nodes 7 and 8, nodes 8 and 9, and nodes 9 and 10 is the same as Eqs .(1)-(3) and Eqs. (7)-(9).

As derived in Appendix C, for a two chamber muffler connected with four parallel dissipative tubes, the four-pole matrices between nodes 5a and 6a, 5b and 6b, 5c and 6c, and 5d and 6d nodes can be combined into an equivalent matrix

$$\begin{bmatrix} p_5 \\ \rho_o c_o u_5 \end{bmatrix} = \begin{bmatrix} TPW1_{1,1} & \frac{1}{4} \cdot TPW1_{1,2} \\ 4 \cdot TPW1_{2,1} & TPW1_{2,2} \end{bmatrix} \begin{bmatrix} p_6 \\ \rho_o c_o u_6 \end{bmatrix} \tag{15}$$

where $[TPW1_{i,j}]$ is the four-pole matrix for a single dissipative tube.

The related equivalent acoustical field of muffler C is also presented and shown in Fig. 4. Consequently, the total transfer matrix assembled by multiplication is

$$\begin{pmatrix} p_1 \\ \rho_o c_o u_1 \end{pmatrix} = f_1(L_i, D_i, M_i) f_2(L_i, D_i, M_i) f_3(L_i, D_i, M_i) f_4(L_i, D_i, M_i) f_5(L_i, D_i, M_i)$$
$$\begin{bmatrix} TS1_{1,1} & TS1_{1,2} \\ TS1_{2,1} & TS1_{2,2} \end{bmatrix} \begin{bmatrix} TSE1_{1,1} & TSE1_{1,2} \\ TSE1_{2,1} & TSE1_{2,2} \end{bmatrix} \begin{bmatrix} TS2_{1,1} & TS2_{1,2} \\ TS2_{2,1} & TS2_{2,2} \end{bmatrix} \begin{bmatrix} TSC1_{1,1} & TSC1_{1,2} \\ TSC1_{2,1} & TSC1_{2,2} \end{bmatrix}$$
$$\begin{bmatrix} TPW1_{1,1} & \frac{1}{4} \cdot TPW1_{1,2} \\ 4 \cdot TPW1_{2,1} & TPW1_{2,2} \end{bmatrix} \begin{bmatrix} TSE2_{1,1} & TSE2_{1,2} \\ TSE2_{2,1} & TSE2_{2,2} \end{bmatrix} \begin{bmatrix} TS3_{1,1} & TS3_{1,2} \\ TS3_{2,1} & TS3_{2,2} \end{bmatrix} \begin{bmatrix} TSC2_{1,1} & TSC2_{1,2} \\ TSC2_{2,1} & TSC2_{2,2} \end{bmatrix}$$
$$\begin{bmatrix} TS4_{1,1} & TS4_{1,2} \\ TS4_{2,1} & TS4_{2,2} \end{bmatrix} \begin{pmatrix} p_{10} \\ \rho_o c_o u_{10} \end{pmatrix} \tag{16}$$

A simplified form is expressed in a matrix as

$$\begin{pmatrix} p_1 \\ \rho_o c_o u_1 \end{pmatrix} = \begin{bmatrix} T_{11}^{***} & T_{12}^{***} \\ T_{21}^{***} & T_{22}^{***} \end{bmatrix} \begin{pmatrix} p_{10} \\ \rho_o c_o u_{10} \end{pmatrix} \tag{17}$$

4. Overall Sound Power Level

The sound transmission loss (*STL*) of mufflers A-C are defined as (Munjal, 1987)

$$STL_1(Q, f, RT_1, RT_2, RT_3, RT_4, RT_5, RT_6, RT_7) = 20\log\left(\frac{\left|T_{11}^{*} + T_{12}^{*} + T_{21}^{*} + T_{22}^{*}\right|}{2}\right) + 10\log\left(\frac{S_1}{S_{10}}\right) \tag{18a}$$

$$STL_2(Q, f, RT_1, RT_2, RT_3, RT_4, RT_5, RT_6, RT_7) = 20\log\left(\frac{\left|T_{11}^{**} + T_{12}^{**} + T_{21}^{**} + T_{22}^{**}\right|}{2}\right) + 10\log\left(\frac{S_1}{S_{10}}\right) \tag{18b}$$

$$STL_3(Q, f, RT_1, RT_2, RT_3, RT_4, RT_5, RT_6, RT_7) = 20\log\left(\frac{\left|T_{11}^{***} + T_{12}^{***} + T_{21}^{***} + T_{22}^{***}\right|}{2}\right) + 10\log\left(\frac{S_1}{S_{10}}\right) \tag{18c}$$

The silenced octave sound power level emitted from a muffler's outlet is

$$SWL_i = SWLO(f_i) - STL(f_i) \tag{19}$$

where

(1) $SWLO(f_i)$ is the original *SWL* at the inlet of a muffler (or pipe outlet), and f_i is the relative octave band frequency.
(2) $STL(f_i)$ is the muffler's *STL* with respect to the relative octave band frequency (f_i).
(3) SWL_i is the silenced *SWL* at the outlet of a muffler with respect to the relative octave band frequency.

Finally, the overall SWL_T silenced by a muffler at the outlet is

$$SWL_{T-K} = 10 * \log\{\sum_{i=1}^{n} 10^{SWL_i/10}\}$$
$$= 10 * \log\left\{10^{\frac{[SWLO(f_1)-}{STL_K(f_1)]/10}} + 10^{\frac{[SWLO(f_2)-}{STL_K(f_2)]/10}} + 10^{\frac{[SWLO(f_3)-}{STL_K(f_3)]/10}} + \ldots + 10^{\frac{[SWLO(f_n)-}{STL_K(f_n)]/10}}\right\} \tag{20}$$

5. Objective Function

1) STL Maximization for a Tone (f) Noise

For muffler A (a two-chamber muffler hybridized with one dissipative duct), the objective function in maximizing the STL at a pure tone (*f*) is

$$OBJ_{11} = STL_1(Q, f, RT_1, RT_2, RT_3, RT_4, RT_5, RT_6, RT_7) \tag{21a}$$

where

RT1=D2; RT2=D3/D2; RT3=D4;
RT4=L3; RT5=dH; RT6=η; RT7=σ (21b)

The related ranges of the parameters are

Q=0.005 (m3/s); Lo =1.0(m); Do=0.4(m); L1=0.05(m);
L5=0.05(m); D1=0.2(m);
RT1:[0.1,0.25]; RT2:[0.3,0.7]; RT3:[0.1,0.5]; RT4:[0.3,0.5];
RT5:[0.00175,0.007]; RT6:[0.01,0.3]; RT7:[3000,20000] (21c)

2) SWL Minimization for a Broadband Noise

To minimize the overall SWL_T, the objective functions for muffler A-C are

$$OBJ_{21} = SWL_{T-1}(Q, RT_1, RT_2, RT_3, RT_4, RT_5, RT_6, RT_7) \tag{22a}$$

$$OBJ_{22} = SWL_{T-2}(Q, RT_1, RT_2, RT_3, RT_4, RT_5, RT_6, RT_7) \tag{22b}$$

$$OBJ_{23} = SWL_{T-3}(Q, RT_1, RT_2, RT_3, RT_4, RT_5, RT_6, RT_7) \tag{22c}$$

IV. MODEL CHECK

Before performing the *SA* optimal simulation on mufflers, an accuracy check of the mathematical model on the acoustical

Table 1. Unsilenced *SWL* of a fan inside a duct outlet.

F (Hz)	125	250	500	1 k	2 k	overall
SWL-dB (A)	85	98	108	116	100	112

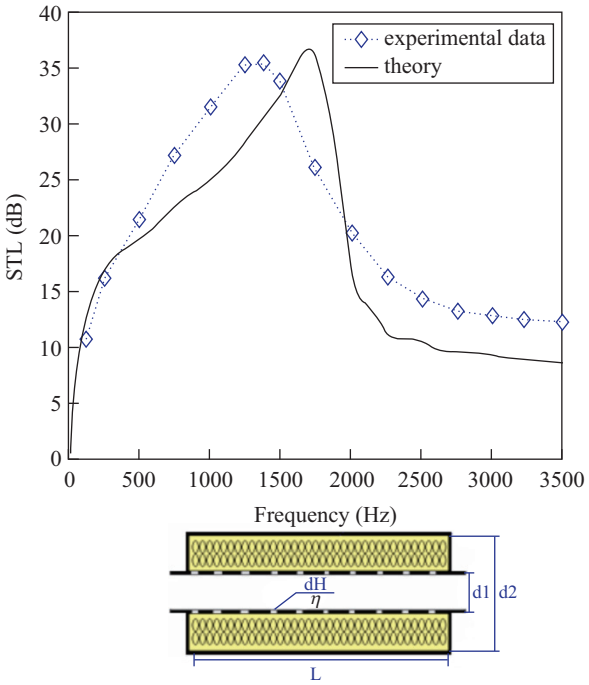

Fig. 5. Performance of an acoustical element with a dissipative duct without the mean flow [L = 0.2572 (m); d1 = 0.00049 (m); d2 = 0.001644 (m); η = 8.4%; dH = 0.00498 (m) ;density = 100 (kg/m3); M = 0] [Experimental data is from Lee (2005)].

elements of a dissipative duct (IV) is performed using the experimental data from Lee (2005). As depicted in Fig. 5, the peak of the theoretical curve is shifted a little to the right; however, the trend of the profiles are similar. Overall, the theoretical and experimental data are roughly in agreement. Therefore, the proposed fundamental mathematical model for the dissipative tube could be acceptable. Consequently, the model linked with the numerical method is applied to the shape optimization in the following section.

V. CASE STUDIES

The noise reduction of a venting system within a space-constrained room is introduced and shown in Fig. 1. The sound power level (*SWL*) inside the venting system's outlet is shown in Table 1 where the overall *SWL* reaches 112 dB. It is obvious that the noise levels at the higher frequencies (500 Hz ~ 2000 Hz) are remarkably high (100~116 dB). To efficiently reduce the venting noise emitted from the venting system, a hybrid muffler having reactive acoustical elements and dissipative acoustical elements is necessary. Here, three types of two-chamber mufflers hybridized and connected with multiple parallel dissipative tubes (mufflers A-C) that disperse venting fluid and decrease the secondary flowing noise are considered.

To obtain the best acoustical performance within a fixed space, numerical assessments linked to an *SA* optimizer are applied. Before the minimization of a broadband noise is performed, a reliability check of the *SA* method by maximization of the *STL* at a targeted tone (400 Hz) is performed. As shown in Fig. 1, the available space for a muffler is 0.4 m in width, 0.4 m in height, and 1.0 m in length. The flow rate (Q) and thickness of a perforated tube (t) are preset at 0.005 (m^3/s) and 0.001 (m), respectively. The corresponding *OBJ* functions, space constraints, and ranges of the design parameters are summarized in Eqs. (23) and (24).

VI. SIMULATED ANNEALING METHOD

For two decades now, there has been a concerted effort to develop Evolutionary Algorithms (*EA*s) that efficiently search for appropriate global solutions in engineering problems. Currently, it has also been acknowledged that Simulated Annealing (*SA*) is one of the best stochastic search methods. Furthermore, because of the needs of the classical gradient methods *EPFM*, *IPFM* and *FDM* as an appropriate starting point (design data) before optimization is performed, accuracy is limited (Chang et al., 2005). However, before the *SA* is performed, the selection of starting data is obviated. And so, *SA* becomes the adopted optimizer used in the muffler's shape optimization.

First introduced by Metropolis et al. (1953), Simulated Annealing (*SA*) was developed further by Kirkpatrick et al. (1983). Because annealing is the process of heating while simultaneously maintaining a metal at a stabilized temperature as it cools, it allows particles to remain close to the minimal energy state. Generating a random initial solution will start the algorithm. Further, the scheme of *SA* is a variation of the hill-climbing algorithm where all downhill movements for improvement are accepted for the decrement of the system's energy. *SA* also permits movement resulting in inferior solutions (uphill moves) that facilitate an escape from the local optimum. (See Fig. 6 for the *SA* optimization flow diagram.) Now, in order to emulate the *SA*'s evolution, a new random solution (X') is selected from the neighborhood of the current solution (X). If it happens that there is a negative change in the objective function, or energy, ($\Delta F \le 0$), then the resulting solution will be acknowledged as the new current solution with the transition property ($pb(X')$)of 1. However, if there is not a negative change ($\Delta F > 0$), the probability of transitioning to the new state X' will be the function $pb(\Delta F / CT)$. As shown in Eq. (25), the new transition property ($pb(X')$) varied from 0~1 will be calculated using the Boltzmann's factor ($pb(X') = \exp(\Delta F / CT)$) where C and T are the Boltzmann constant and the current temperature.

$$pb(X') = \begin{cases} 1, \Delta F \le 0 \\ \exp(\dfrac{-\Delta F}{CT}), \Delta f > 0 \end{cases} \quad (23a)$$

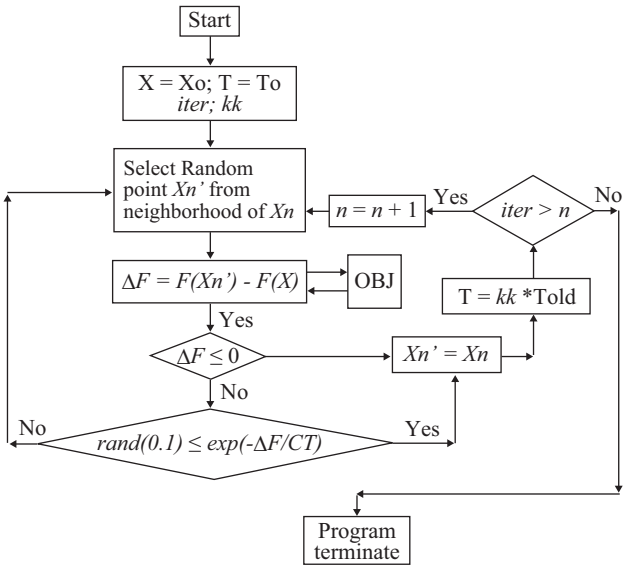

Fig. 6. The flow diagram of the SA optimization.

$$\Delta F = F(X') - F(X) \tag{23b}$$

To escape the local optimum, *SA* also permits movements that result in inferior solutions (uphill moves). Therefore, if the transition property (pb(*X*')) is greater than a random number of rand (0,1), the new inferior solution which results in a higher energy condition will be accepted; otherwise, it will be discarded. Each successful substitution of the new current solution will conduct to the decay of the current temperature as

$$T_{new} = kk * T_{old} \tag{24}$$

where *kk* is the cooling rate.

The process is repeated until the predetermined number (*iter*) of the outer loop is reached.

VII. RESULTS AND DISCUSSION

1. Results

The accuracy of the *SA* optimization depends on two types of *SA* parameters that include *kk* (cooling rate) and *iter* (maximum iteration). To achieve good optimization, the following parameters are varied step by step:

kk(0.91, 0.93, 0.95, 0.97, 0.99); *iter* (25, 50, 100, 500, 1000).

Two results of optimization (one, pure tone noises used for *SA*'s accuracy check; and the other, a broadband noise occurring in a venting system) are described below.

1) Pure Tone Noise Optimization

Before dealing with a broadband noise, the *STL*'s maximization with respect to a one-tone noise (400 Hz) is introduced

Table 2. Optimal *STL* for muffler A (equipped with one perforated dissipative tube) at various *SA* parameters (targeted tone of 400 Hz).

SA parameter		Design parameters							Results
iter	*kk*	RT1	RT2	RT3	RT4	RT5	RT6	RT7	STL_{400Hz} dB
25	0.91	0.1960	0.5561	0.3561	0.4281	0.005111	0.1957	13880	23.9
25	0.93	0.1771	0.5055	0.3055	0.4028	0.004448	0.1590	11740	26.6
25	0.95	0.1672	0.4793	0.2793	0.3897	0.004104	0.1400	10620	27.7
25	0.97	0.1509	0.4358	0.2358	0.3679	0.003533	0.1085	8773	29.0
25	0.99	0.1319	0.3850	0.1850	0.3425	0.002866	0.07163	6613	31.0
50	0.99	0.1188	0.3501	0.1501	0.3251	0.002408	0.04636	5131	33.8
100	0.99	0.1168	0.3449	0.1449	0.3225	0.002339	0.04255	4908	34.5
500	0.99	0.1153	0.3409	0.1409	0.3205	0.002287	0.03967	4739	35.0
1000	0.99	0.1102	0.3271	0.1271	0.3135	0.002106	0.02964	4152	37.3

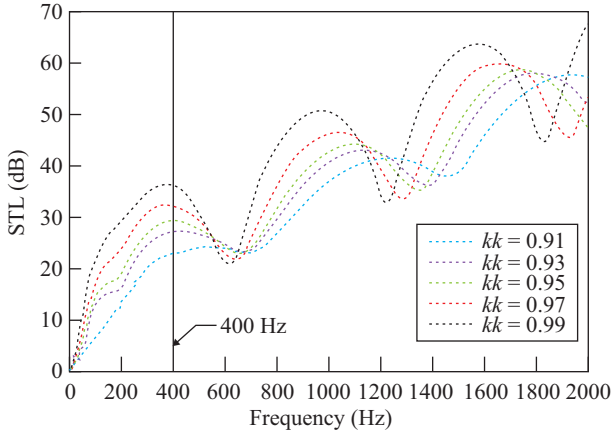

Fig. 7. *STL* with respect to various *kk* [muffler A: *iter* = 25, target tone = 400 Hz].

for a reliability check on the *SA* method. By using Eqs. (23) and (24), the maximization of the *STL* with respect to muffler A (a two-chamber muffler hybridized with one dissipative tube) at the specified pure tone (400 Hz) was performed first. As indicated in Table 2, nine sets of *SA* parameters are tried in the muffler's optimization. Obviously, the optimal design data can be obtained from the last set of *SA* parameters at (*kk, iter*) = (0.99, 1000). Using the optimal design in a theoretical calculation, the optimal *STL* curves with respect to various *SA* parameters (*kk, iter*) are plotted and depicted in Figs. 7 and 8. As revealed in Figs. 7 and 8, the *STL* is precisely maximized at the desired frequency (400 Hz). Consequently, the SA optimizer is reliable in the optimization process.

2) Broadband Noise Optimization

Similarly, considering Eqs. (24a-c) and using the same SA parameters in the broadband optimization process, the minimization of the $SWL_{T\text{-}1}$, $SWL_{T\text{-}2}$, and $SWL_{T\text{-}3}$ with respect to

Table 3. Comparison of the minimized SWLT of three kinds of mufflers (mufflers A-C) [broadband noise].

Muffler Type	Design parameters							Results
	RT1	RT2	RT3	RT4	RT5	RT6	RT7	SWL_T – dB(A)
Muffler A	0.1519	0.4385	0.2385	0.3692	0.003568	0.1104	8885	80.2
Muffler B	0.1519	0.4385	0.2385	0.3692	0.003568	0.1104	8885	84.9
Muffler C	0.1519	0.4385	0.2385	0.3692	0.003568	0.1104	8885	88.5

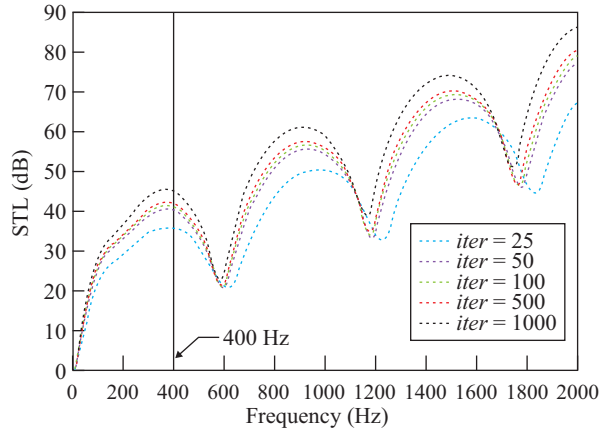

Fig. 8. STL with respect to various *iter* [muffler A: *kk* = 0.99, target tone = 400 Hz].

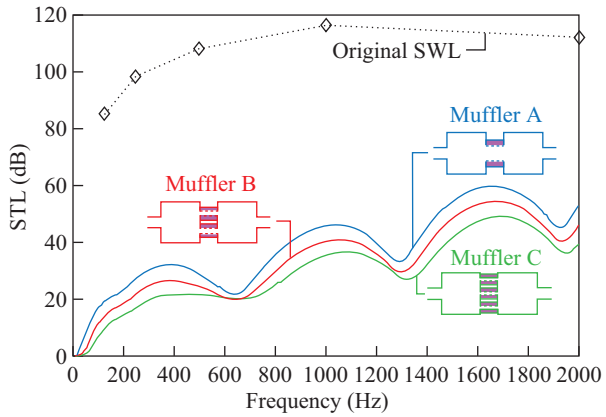

Fig. 9. Comparison of the optimal STLs of three kinds of mufflers (mufflers A, B, and C) and the original SWL.

mufflers A-C was performed and shown in Table 3. As illustrated in Table 3, the resultant sound power levels with respect to three types of mufflers have been reduced from 112 dB to 80.2 dB, 84.9 dB, and 88.5 dB. Using this optimal design in a theoretical calculation, the optimal *STL* curves with respect to various mufflers are plotted and compared with the original *SWL* depicted in Fig. 9.

2. Discussion

In order to decrease the secondary flowing noise generated from the higher speed flow, new muffler designs with multiple parallel dissipative tubes used to disperse the venting fluid are presented. To achieve a sufficient optimization, the selection of the appropriate *SA* parameter set is essential. As indicated in Table 2, the best *SA* set of muffler A at the targeted pure tone noise of 400 Hz has been shown. The related *STL* curves with respect to various *SA* parameters are plotted in Figs. 7 and 8. Figs. 7 and 8 reveal the predicted maximal value of the *STL* is located at the desired frequency.

Table 4. Comparison of the optimal STL for muffler A and muffler D (targeted tone of 400 Hz).

muffler	Design parameters							Results
Muffler A	RT1	RT2	RT3	RT4	RT5	RT6	RT7	STL_{400Hz} dB
	0.1102	0.3271	0.1271	0.3135	0.002106	0.02964	4152	44.3
Muffler D	RT1*	RT2*	RT3*	RT4*	RT5*	RT6*		STL_{400Hz} dB
	0.1042	0.3112	0.1112	0.3056	0.001897	0.01810		47.8

Note:
Muffler A: RT1 = D2; RT2 = D3/D2; RT3 = D4; RT4 = L3; RT5 = dH; RT6 = η; RT7 = σ
Muffler D: RT1* = D2; RT2* = D3; RT3* = D4; RT4* = L3; RT5* = dH; RT6* = η

In dealing with the broadband noise, the acoustical performance among three types of two-chamber mufflers connected with multiple parallel dissipative tubes (mufflers A, B, and C) are shown in Table 3 and Fig. 9. As can be observed in Table 3, the overall sound transmission losses with respect to mufflers A-C are 31.8 dB, 27.1 dB, and 23.5 dB. Results shown in Table 3 and Fig. 9 indicate that the two-chamber muffler hybridized with fewer numbers of parallel dissipative tubes is superior to the other mufflers equipped with more dissipative tubes. It can be seen that for the mufflers equipped with more parallel dissipative tubes, the acoustical performances of the acoustical element (II) between nodes 4 and 5 and acoustical element (III) between nodes 6 and 7 will largely decrease due to the decrement of the area's ratio; therefore, the overall noise reduction of the mufflers with more parallel dissipative tubes will decrease.

To appreciate the acoustical effect of the dissipative tube and the non-dissipative tube (with no wool within the set of perforated tubes), two types of mufflers (mufflers D and E) hybridized with one non-dissipative tube and four parallel non-dissipative tubes shown in Fig 10 are investigated. Using the same *SA* parameters for the pure tone (400 Hz) optimization in muffler D and comparing the related acoustical performance to that of muffler A, the resulting *STL* and acoustical profiles are summarized in Table 4 and plotted in Fig. 11. As indicated in Fig 11, the maximized *STL*s of mufflers A and D are located at the desired frequency (400 Hz). Additionally, the resonating effect of muffler D is better when compared to muffler A. Similarly, using the same *SA* parameters for the

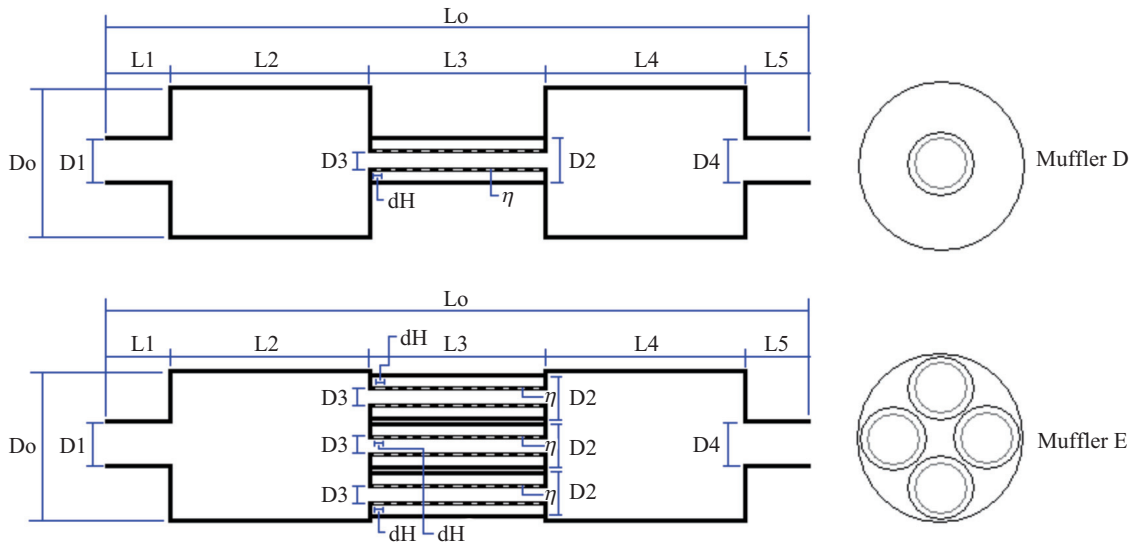

Fig. 10. The outline dimension of multi-perforated-tube mufflers without sound absorbing wool (muffler D and muffler E).

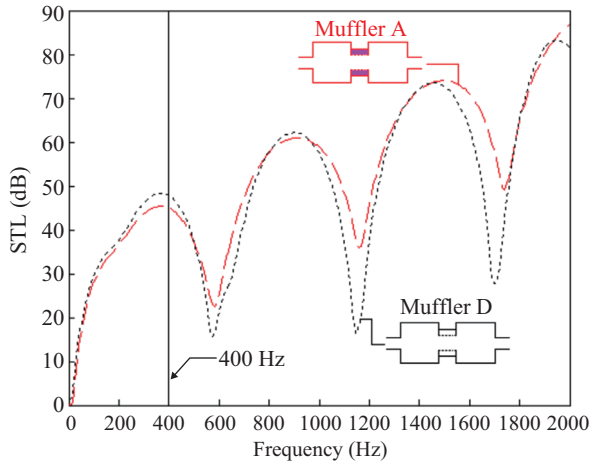

Fig. 11. Comparison of the optimal *STL*s of three kinds of mufflers (mufflers A and D) (optimization at pure tone of 400 Hz).

Table 5. Comparison of the optimal STL for muffler C and muffler E (broadband noise).

muffler	Design parameters							Results
Muffler C	RT1	RT2	RT3	RT4	RT5	RT6	RT7	SWL_T – dB(A)
	0.1519	0.4385	0.2385	0.3692	0.003568	0.1104	8885	88.5
Muffler E	RT1**	RT2**	RT3**	RT4**	RT5**	RT6**		SWL_T – dB(A)
	0.1042	0.3112	0.1112	0.3056	0.001897	0.0181		81.5

Note:
Muffler C: RT1 = D2; RT2 = D3/D2; RT3 = D4; RT4 = L3; RT5 = dH; RT6 = η; RT7 = σ
Muffler E: RT1** = D2; RT2** = D3; RT3** = D4; RT4** = L3;RT5** = dH; RT6** = η

broadband noise elimination in muffler E (with four parallel non-dissipative tubes) and comparing the related acoustical performance to that of muffler C (with four parallel dissipative tubes), the resulting SWL_T and *STL* profiles are summarized in Table 5 and plotted in Fig. 12. As indicated in Fig. 12, the resonating effect of muffler E is much better when compared to muffler C. Consequently, because of the resonating character of the noise reduction, the mufflers (muffler D and muffle E) hybridized with multiple parallel non-dissipative tubes (with no wool within the set of a perforated tube) are suitable in dealing with the multi- tone noise wave. However, because mufflers A-C (hybridized with multiple parallel dissipative tubes) have a wider *STL* curve and with the *STL* performing better at the higher frequencies, they are suitable for dealing with the middle and higher broadband noise.

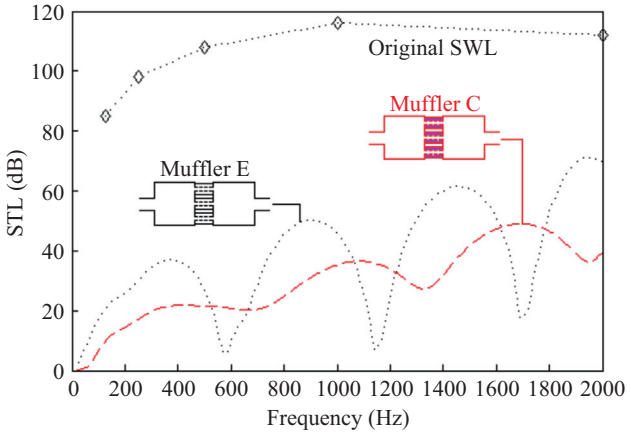

Fig. 12. Comparison of the optimal STLs of three kinds of mufflers (mufflers C and E) and the original SWL.

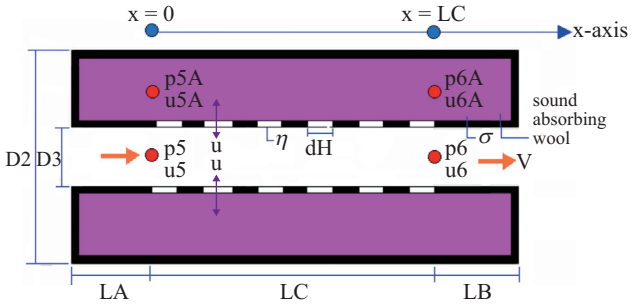

Fig. 13. Acoustical field of a perforated dissipative tube filled with sound absorbing wool.

VIII. CONCLUSION

It has been shown that two-chamber mufflers hybridized with multiple parallel dissipative tubes can be easily and efficiently optimized within a limited space by using a decoupling technique, a plane wave theory, a four-pole transfer matrix, and a *SA* optimizer. As indicated in Table 3 and Figs. 7 and 8, two kinds of *SA* parameters (*kk* and *iter*) play essential roles in the solution's accuracy during *SA* optimization. Figs. 7 and 8 indicate that the tuning ability established by adjusting design parameters of muffler A is reliable.

Additionally, the appropriate acoustical performance curve of the three types of two-chamber mufflers hybridized with multiple parallel dissipative tubes (mufflers A-C) has been assessed. As indicated in Table 3 and Fig. 9, the resultant SWL_T with respect to these mufflers is 80.2 dB, 84.9 dB, and 88.5 dB. Obviously, the muffler hybridized with fewer number of parallel dissipative tubes is superior to the other mufflers equipped with more parallel dissipative tubes. It can be seen that more dissipative tubes installed between the two-chamber muffler will disperse the venting fluid and reduce the secondary noise; however, the acoustical performances of the acoustical element (II) between nodes 4 and 5 and the acoustical element (III) between nodes 6 and 7 will decrease even though the number of parallel dissipative tubes for the muffler increases. Moreover, as investigated in Section 7.2, because of the resonating character of noise reduction, the mufflers (muffler D and E) having multiple parallel non-dissipative tubes (with no wool within the set of a perforated tube) are excellent for dealing with a multiple tone noise wave. On the other hand, the mufflers (mufflers A-C) hybridized with multiple parallel dissipative tubes (with wool within the set of perforated tubes) are suitable for dealing with the middle and higher broadband noise.

ACKNOWLEDGEMENTS

The authors acknowledge the financial support of the National Science Council (NSC 99-2622-E-235-002-CC3 and NSC 102-2622-E-235-001-CC3, ROC).

NOMENCLATURE

This paper is constructed on the basis of the following notations:

c_o: sound speed (ms^{-1})
$\tilde{c}$: sound speed in a wool (ms^{-1})
dH_i: the diameter of a perforated hole on the *i*-th inner tube (m)
D_i: diameter of the *i*-th perforated tubes (m)
D_o: diameter of the outer tube (m)
f: cyclic frequency (Hz)
ff_i: coefficients in function ($\Gamma_i = ff_i e^{\beta_i x}$)
iter: maximum iteration
j: imaginary unit
k: wave number ($= \frac{\omega}{c_o}$)
$\tilde{k}$: the wave number for the wool
kk: cooling rate in *SA*
L_o: total length of the muffler (m)
M: mean flow Mach number
OBJ: objective function (dB)
p: acoustic pressure (Pa)
p_i: acoustic pressure at the *i*-th node (Pa)
pb(T): transition probability
Q: volume flow rate of venting gas (m^3s^{-1})
RT_i: the design parameters of the mufflers
S_i: section area at the *i*-th node(m^2)
STL: sound transmission loss (dB)
SWL_O: unsilenced sound power level inside the muffler's inlet (dB)
SWL_T: overall sound power level inside the muffler's output (dB)
t: the thickness of the inner perforated tube (m)
TS_{ij}: components of four-pole transfer matrices for an acoustical mechanism with straight ducts
TSC_{ij}: components of four-pole transfer matrices for an acoustical mechanism with sudden contraction ducts
TSE_{ij}: components of four-pole transfer matrices for an acoustical mechanism with sudden expansion ducts
TPW_{ij}: components of a four-pole transfer matrix for an acoustical mechanism with a dissipative tube
T: current temperature (°C)

T^*_{ij}: components of a four-pole transfer system matrix
T_o: initial temperature (°C)
u_i: acoustic particle velocity at the i-th node (ms^{-1})
u: acoustical particle velocity passing through a perforated hole from the i-th node to the j-th node (ms^{-1})
V: mean flow velocity at the perforated tube (ms^{-1})
ρ_o: air density (kg m^{-3})
ρ: wool density (kg m^{-3})
ρ_i: acoustical density at the i-th node (kg m^{-3})
ξ_i: specific acoustical impedance of the i-th inner perforated tube
η_i: the porosity of the i-th inner perforated tube.
σ: the acoustical flowing resistance for the wool (rayls/m)
β_i: i-th eigen value of $[M]_{4x4}$
ω: angular velocity (= $2\pi f$)
$[\Pi]_{4x4}$: the model matrix formed by four sets of eigen vectors Π_{4x1} of $[M]_{4x4}$.

APPENDIX A

Transfer Matrix of a Perforated Chamber Filled with Sound Absorbing Wool

As indicated in Fig. 13, the perforated resonator is composed of an inner perforated tube and an outer resonating chamber. Based on Sullivan and Crocker's derivation (1978), the continuity equations and momentum equations with respect to inner and outer tubes at nodes 5 and 5a are listed below.

Inner Tube:

continuity equation:

$$V\frac{\partial \rho_5}{\partial x}+\rho_o\frac{\partial u_5}{\partial x}+\frac{4\rho_o}{D_3}u+\frac{\partial \rho_5}{\partial t}=0 \tag{A1}$$

momentum equation:

$$\rho_o\left(\frac{\partial}{\partial t}+V\frac{\partial}{\partial x}\right)u_5+\frac{\partial p_5}{\partial x}=0 \tag{A2}$$

Outer Tube:

continuity equation:

$$\rho\frac{\partial u_{5A}}{\partial x}-\frac{4D_3\rho}{D_2^2-D_3^2}u+\frac{\partial \rho_{5A}}{\partial t}=0 \tag{A3}$$

momentum equation

$$\rho\frac{\partial u_{5A}}{\partial t}+\frac{\partial p_{5A}}{\partial x}=0 \tag{A4}$$

Assuming that the acoustic wave is a harmonic motion

$$p(x,t)=P(x)\cdot e^{j\omega t} \tag{A5}$$

under the isentropic processes in ducts, it yields

$$P(x)=\rho(x)\cdot c_o^2 \tag{A6}$$

Assuming that the perforation along the inner tube is uniform ($d\xi/dx=0$), the acoustic impedance of the perforation ($\rho_o c_o \xi$) is

$$\rho_o c_o \xi=\frac{p_5(x)-p_{5A}(x)}{u(x)} \tag{A7}$$

where ξ is the specific acoustical impedance of the perforated tube.

The empirical formulations developed by Sullivan (1978) and Rao & Munjal (1984) for the perforates with and without mean flow are adopted in this study.

For perforates with a stationary medium, we have

$$\xi=[0.006+jk(t+0.75dH)]/\eta \tag{A8a}$$

For perforates with grazing flow, we have

$$\xi=[0.514D_3M/(L_C\eta)+j0.95k(t+0.75dH)]/\eta \tag{A8b}$$

where dH is the diameter of a perforated hole on the inner tube, t is the thickness of an inner perforated tube, and η is the porosity of the perforated tube.

Plugging Eqs. (A5)-(A7) into Eqs. (A1)-(A4) and eliminating u_5 and u_{5A}, we have

$$\left[\left(1-M^2\right)\frac{d^2}{dx^2}-2jMk\frac{d}{dx}+k^2\right]p_5-\frac{4}{D_3\xi}\left[M\frac{d}{dx}+jk\right]\left(p_5-p_{5A}\right)=0 \tag{A9}$$

$$\left[\frac{d^2}{dx^2}+\tilde{k}^2\right]p_{5A}+j\frac{4kD_3\tilde{\rho}}{(D_2^2-D_3^2)\xi\rho_0}\left(p_5-p_{5A}\right)=0 \tag{A10}$$

where $M=\dfrac{V}{c_o}$

Alternatively, Eqs. (A9) and (A10) can be expressed as

$$p_5''+\alpha\alpha_1 p_5'+\alpha\alpha_2 p_5+\alpha\alpha_3 p_{5A}'+\alpha\alpha_4 p_{5A}=0 \tag{A11a}$$

$$\alpha\alpha_5 p_5'+\alpha\alpha_6 p_5+p_{5A}''+\alpha\alpha_7 p_{5A}'+\alpha\alpha_8 p_{5A}=0 \tag{A11b}$$

where

$$\alpha\alpha_1 = -\frac{jM}{1-M^2}\left(2k - j\frac{4}{D_3\xi}\right);$$

$$\alpha\alpha_2 = \frac{1}{1-M^2}\left(k^2 - j\frac{4k}{D_3\xi}\right);$$

$$\alpha\alpha_3 = \frac{M}{1-M^2}\cdot\frac{4}{D_3\xi};$$

$$\alpha\alpha_4 = \frac{j}{1-M^2}\cdot\frac{4k}{D_3\xi};$$

$$\alpha\alpha_5 = 0;$$

$$\alpha\alpha_6 = \frac{j4kD_3\tilde{\rho}}{(D_2^2 - D_3^2)\xi\rho_o};$$

$$\alpha\alpha_7 = 0;$$

$$\alpha\alpha_8 = \tilde{k}^2 - \frac{j4kD_3\tilde{\rho}}{(D_2^2 - D_3^2)\xi\rho_o};$$

$$k = \frac{\omega}{c}; \qquad \text{(A11c)}$$

Let

$$p_5^{'} = \frac{dp_5}{dx} = y_1,\ p_{5A}^{'} = \frac{dp_{5A}}{dx} = y_2,\ p_5 = y_3,\ p_{5A} = y_4 \qquad \text{(A12)}$$

According to Eqs. (A11) and (A12), the new matrix between {y'} and {y} is

$$\begin{bmatrix} y_1^{'} \\ y_2^{'} \\ y_3^{'} \\ y_4^{'} \end{bmatrix} = \begin{bmatrix} -\alpha\alpha_1 & -\alpha\alpha_3 & -\alpha\alpha_2 & -\alpha\alpha_4 \\ -\alpha\alpha_5 & -\alpha\alpha_7 & -\alpha\alpha_6 & -\alpha\alpha_8 \\ 1 & 0 & 0 & 0 \\ 0 & 1 & 0 & 0 \end{bmatrix} \begin{bmatrix} y_1 \\ y_2 \\ y_3 \\ y_4 \end{bmatrix} \qquad \text{(A13a)}$$

which can be briefly expressed as

$$\{y^{'}\} = [\mathrm{M}]\{y\} \qquad \text{(A13b)}$$

Let

$$\{y\} = [\Pi]\{\Gamma\} \qquad \text{(A14a)}$$

which is

$$\begin{bmatrix} dp_5/dx \\ dp_{5A}/dx \\ p_5 \\ p_{5A} \end{bmatrix} = \begin{bmatrix} \Pi_{1,1} & \Pi_{1,2} & \Pi_{1,3} & \Pi_{1,4} \\ \Pi_{2,1} & \Pi_{2,2} & \Pi_{2,3} & \Pi_{2,4} \\ \Pi_{3,1} & \Pi_{3,2} & \Pi_{3,3} & \Pi_{3,4} \\ \Pi_{4,1} & \Pi_{4,2} & \Pi_{4,3} & \Pi_{4,4} \end{bmatrix} \begin{bmatrix} \Gamma_1 \\ \Gamma_2 \\ \Gamma_3 \\ \Gamma_4 \end{bmatrix} \qquad \text{(A14b)}$$

$[\Pi]_{4x4}$ is the model matrix formed by four sets of eigen vectors Π_{4x1} of $[\mathrm{M}]_{4x4}$.

Combining Eq. (A14) with (A13) and then multiplying $[\Pi]^{-1}$ by both sides yields

$$[\Pi]^{-1}[\Pi]\{\Gamma^{'}\} = [\Pi]^{-1}[\mathrm{M}][\Pi]\{\Gamma\} \qquad \text{(A15a)}$$

Set

$$[\Psi] = [\Pi]^{-1}[\mathrm{M}][\Pi] = \begin{bmatrix} \beta_1 & 0 & 0 & 0 \\ 0 & \beta_2 & 0 & 0 \\ 0 & 0 & \beta_3 & 0 \\ 0 & 0 & 0 & \beta_4 \end{bmatrix} \qquad \text{(A15b)}$$

where β_i is the eigen value of [M].

Eq. (A13) can be rewritten as

$$\{\Gamma^{'}\} = [\Psi]\{\Gamma\} \qquad \text{(A16)}$$

Obviously, Eq. (A15) is a decoupled equation. The related solution obtained is

$$\Gamma_i = ff_i e^{\beta_i x} \qquad \text{(A17)}$$

Plugging Eq. (A17) into (A14b) and rearranging them, we have

$$\begin{bmatrix} p_5(x) \\ p_{5A(x)} \\ \dfrac{dp_5(x)}{dx} \\ \dfrac{dp_{5A}(x)}{dx} \end{bmatrix} = \begin{bmatrix} \Pi_{3,1}e^{r_1 x} & \Pi_{3,2}e^{r_2 x} & \Pi_{3,3}e^{r_3 x} & \Pi_{3,4}e^{r_4 x} \\ \Pi_{4,1}e^{r_1 x} & \Pi_{4,2}e^{r_2 x} & \Pi_{4,3}e^{r_3 x} & \Pi_{4,4}e^{r_4 x} \\ \Pi_{1,1}e^{r_1 x} & \Pi_{1,2}e^{r_2 x} & \Pi_{1,3}e^{r_3 x} & \Pi_{1,4}e^{r_4 x} \\ \Pi_{2,1}e^{r_1 x} & \Pi_{2,2}e^{r_2 x} & \Pi_{2,3}e^{r_3 x} & \Pi_{2,4}e^{r_4 x} \end{bmatrix} \begin{bmatrix} ff_1 \\ ff_2 \\ ff_3 \\ ff_4 \end{bmatrix} \qquad \text{(A18)}$$

Eqs. (A2) and (A4) become

$$\rho_o c_o u_5 = -\frac{1}{jk + M\beta_i}\frac{dp_5}{dx};$$

$$\tilde{\rho}\tilde{c}u_{5A} = -\frac{1}{j\tilde{k}}\frac{dp_{5A}}{dx} \qquad \text{(A19)}$$

Plugging Eq. (A19) into (A18) yields

$$\begin{bmatrix} p_5(x) \\ p_{5A}(x) \\ \rho_o c_o u_5(x) \\ \tilde{\rho}\tilde{c}u_{5A}(x) \end{bmatrix} = \begin{bmatrix} \Lambda_{1,1} & \Lambda_{1,2} & \Lambda_{1,3} & \Lambda_{1,4} \\ \Lambda_{2,1} & \Lambda_{2,2} & \Lambda_{2,3} & \Lambda_{2,4} \\ \Lambda_{3,1} & \Lambda_{3,2} & \Lambda_{3,3} & \Lambda_{3,4} \\ \Lambda_{4,1} & \Lambda_{4,2} & \Lambda_{4,3} & \Lambda_{4,4} \end{bmatrix} \begin{bmatrix} ff_1 \\ ff_2 \\ ff_3 \\ ff_4 \end{bmatrix} \qquad \text{(A20)}$$

Substituting two cases of $x = 0$ and $x = Lc$ into Eq. (A20) yields

$$\begin{bmatrix} p_5(0) \\ p_{5A}(0) \\ \rho_o c_o u_5(0) \\ \tilde{\rho}\tilde{c}u_{5A}(0) \end{bmatrix} = [\Theta] \begin{bmatrix} p_5(L_C) \\ p_{5A}(L_C) \\ \rho_o c_o u_5(L_C) \\ \rho c u_{5A}(L_C) \end{bmatrix} \quad \text{(A21a)}$$

where

$$[\Theta] = [\Lambda(0)][\Lambda(L_C)]^{-1} \quad \text{(A21b)}$$

The boundary conditions for the inner tube are

$$\frac{p_{5A}(0)}{-u_{5A}(0)} = -j\tilde{\rho}\tilde{c}\cot(\tilde{k}L_A) \text{ at } x = 0 \quad \text{(A22a)}$$

$$\frac{p_{5A}(L_C)}{u_{5A}(L_C)} = -j\tilde{\rho}\tilde{c}\cot(\tilde{k}L_B) \text{ at } x = L_C \quad \text{(A22b)}$$

Plugging Eq. (A22) into (A21) yields

$$\begin{bmatrix} p_5(0) \\ \rho_o c_o u_5(0) \end{bmatrix} = \begin{bmatrix} TPW_{1,1} & TPW_{1,2} \\ TPW_{2,1} & TPW_{2,2} \end{bmatrix} \begin{bmatrix} p_{5A}(L_C) \\ \rho_o c_o u_{5A}(L_C) \end{bmatrix} \quad \text{(A23a)}$$

The simplified alternative form is

$$\begin{bmatrix} p_5 \\ \rho_o c_o u_5 \end{bmatrix} = \begin{bmatrix} TPW_{1,1} & TPW_{1,2} \\ TPW_{2,1} & TPW_{2,2} \end{bmatrix} \begin{bmatrix} p_6 \\ \rho_o c_o u_6 \end{bmatrix} \quad \text{(A23b)}$$

where

$$\bar{p}_5 = p_5(0)\ ;\ u_5 = u_5(0)\ ;\ p_6 = p_{5A}(L_C)\ ;\ u_6 = u_{5A}(L_C) \quad \text{(A23c)}$$

APPENDIX B

Transfer Matrix of Two Parallel Dissipative Tubes

As indicated in Fig. 2 and Appendix A, the acoustical four-pole matrix between node 5a and 6a for muffler B is

$$\begin{bmatrix} p_{5a} \\ \rho_o c_o u_{5a} \end{bmatrix} = \begin{bmatrix} TPW1_{1,1} & TPW1_{1,2} \\ TPW1_{2,1} & TPW1_{2,2} \end{bmatrix} \begin{bmatrix} p_{6a} \\ \rho_o c_c u_{6a} \end{bmatrix} \quad \text{(B1)}$$

Developing Eq. (B1) yields

$$p_{5a} = TPW1_{1,1} \cdot p_{6a} + TPW1_{1,2} \cdot \rho_o c_c u_{6a} \quad \text{(B2a)}$$

$$\rho_o c_o u_{5a} = TPW1_{2,1} \cdot p_{6a} + TPW1_{2,2} \cdot \rho_o c_c u_{6a} \quad \text{(B2b)}$$

Similarly, the acoustical four-pole matrix between node 5b and 6b is

$$\begin{bmatrix} p_{5b} \\ \rho_o c_o u_{5b} \end{bmatrix} = \begin{bmatrix} TPW1_{1,1} & TPW1_{1,2} \\ TPW1_{2,1} & TPW1_{2,2} \end{bmatrix} \begin{bmatrix} p_{6b} \\ \rho_o c_o u_{6b} \end{bmatrix} \quad \text{(B3)}$$

Developing Eq. (B3) yields

$$p_{5b} = TPW1_{1,1} \cdot p_{6b} + TPW1_{1,2} \cdot \rho_o c_c u_{6b} \quad \text{(B4a)}$$

$$\rho_o c_o u_{5b} = TPW1_{2,1} \cdot p_{6b} + TPW1_{2,2} \cdot \rho_o c_c u_{6b} \quad \text{(B4b)}$$

Combining Eq. (B2a) and Eq. (B4a) yields

$$p_{5a} + p_{5b} = TPW1_{1,1} \cdot [p_{6a} + p_{6b}] + TPW1_{1,2} \cdot \rho_o c_c [u_{6a} + u_{6b}] \quad \text{(B5)}$$

Likewise, combining Eq. (B2b) and Eq. (B4b) yields

$$\rho_o c_o [u_{5a} + u_{5b}] = TPW1_{2,1} \cdot [p_{6a} + p_{6b}] + TPW1_{2,2} \cdot \rho_o c_c [u_{6a} + u_{6b}] \quad \text{(B6)}$$

where

$$p_5 = p_{5a} = p_{5b};\ p_6 = p_{6a} = p_{6b};\ u_5 = u_{5a} + u_{5b};\ u_6 = u_{6a} + u_{6b} \quad \text{(B7)}$$

Plugging Eq. (B7) into Eqs. (B5) and (B6) yields

$$2 \cdot p_5 = 2 \cdot TPW1_{1,1} \cdot p_6 + TPW1_{1,2} \cdot \rho_o c_c u_6 \quad \text{(B8a)}$$

$$\rho_o c_o u_5 = 2 \cdot TPW1_{2,1} \cdot p_6 + TPW1_{2,2} \cdot \rho_o c_c u_6 \quad \text{(B8b)}$$

Rearranging Eq. (B8) in a matrix form, the equivalent four-pole matrix between nodes 5 and 6 shown in Fig. 4 is

$$\begin{bmatrix} p_5 \\ \rho_o c_o u_5 \end{bmatrix} = \begin{bmatrix} TPW1_{1,1} & \frac{1}{2} \cdot TPW1_{1,2} \\ 2 \cdot TPW1_{2,1} & TPW1_{2,2} \end{bmatrix} \begin{bmatrix} p_6 \\ \rho_o c_o u_6 \end{bmatrix} \quad \text{(B9)}$$

APPENDIX C

Transfer Matrix of Four Parallel Dissipative Tubes

As indicated in Fig. 2, muffler C's acoustical four-pole matrix between node 5a and 6a is

$$\begin{bmatrix} p_{5a} \\ \rho_o c_o u_{5a} \end{bmatrix} = \begin{bmatrix} TPW1_{1,1} & TPW1_{1,2} \\ TPW1_{2,1} & TPW1_{2,2} \end{bmatrix} \begin{bmatrix} p_{6a} \\ \rho_o c_o u_{6a} \end{bmatrix} \quad \text{(C1)}$$

Developing Eq. (C1) yields

$$p_{5a} = TPW1_{1,1} \cdot p_{6a} + TPW1_{1,2} \cdot \rho_o c_c u_{6a} \quad \text{(C2a)}$$

$$\rho_o c_o u_{5a} = TPW1_{2,1} \cdot p_{6a} + TPW1_{2,2} \cdot \rho_o c_c u_{6a} \quad \text{(C2b)}$$

Similarly, the acoustical four-pole matrices between node 5b and 6b, node 5c and 6c, and node 5d and 6d are

$$\begin{bmatrix} p_{5b} \\ \rho_o c_o u_{5b} \end{bmatrix} = \begin{bmatrix} TPW1_{1,1} & TPW1_{1,2} \\ TPW1_{2,1} & TPW1_{2,2} \end{bmatrix} \begin{bmatrix} p_{6b} \\ \rho_o c_o u_{6b} \end{bmatrix} \quad \text{(C3a)}$$

$$\begin{bmatrix} p_{5c} \\ \rho_o c_o u_{5c} \end{bmatrix} = \begin{bmatrix} TPW1_{1,1} & TPW1_{1,2} \\ TPW1_{2,1} & TPW1_{2,2} \end{bmatrix} \begin{bmatrix} p_{6c} \\ \rho_o c_o u_{6c} \end{bmatrix} \quad \text{(C3b)}$$

$$\begin{bmatrix} p_{5d} \\ \rho_o c_o u_{5d} \end{bmatrix} = \begin{bmatrix} TPW1_{1,1} & TPW1_{1,2} \\ TPW1_{2,1} & TPW1_{2,2} \end{bmatrix} \begin{bmatrix} p_{6d} \\ \rho_o c_o u_{6d} \end{bmatrix} \quad \text{(C3c)}$$

Developing Eqs. (C3a)-(C3c) yields

$$p_{5b} = TPW1_{1,1} \cdot p_{6b} + TPW1_{1,2} \cdot \rho_o c_c u_{6b} \quad \text{(C4a)}$$

$$\rho_o c_o u_{5b} = TPW1_{2,1} \cdot p_{6b} + TPW1_{2,2} \cdot \rho_o c_c u_{6b} \quad \text{(C4b)}$$

$$p_{5c} = TPW1_{1,1} \cdot p_{6c} + TPW1_{1,2} \cdot \rho_o c_c u_{6c} \quad \text{(C4c)}$$

$$\rho_o c_o u_{5c} = TPW1_{2,1} \cdot p_{6c} + TPW1_{2,2} \cdot \rho_o c_c u_{6c} \quad \text{(C4d)}$$

$$p_{5d} = TPW1_{1,1} \cdot p_{6d} + TPW1_{1,2} \cdot \rho_o c_c u_{6d} \quad \text{(C4e)}$$

$$\rho_o c_o u_{5d} = TPW1_{2,1} \cdot p_{6d} + TPW1_{2,2} \cdot \rho_o c_c u_{6d} \quad \text{(C4f)}$$

Combining Eq. (C2a) and Eq. (C4a), (C4c), and (C4e) yields

$$\begin{aligned} p_{5a} + p_{5b} + p_{5c} + p_{5d} &= TPW1_{1,1} \cdot [p_{6a} + p_{6b} + p_{6c} + p_{6d)}] \\ &+ TPW1_{1,2} \cdot \rho_o c_c [u_{6a} + u_{6b} + u_{6c} + u_{6d}] \end{aligned} \quad \text{(C5)}$$

Likewise, combining Eq. (C2b) and Eq. (C4b), (C4d), and (C4f) yields

$$\begin{aligned} \rho_o c_o [u_{5a} + u_{5b} + u_{5c} + u_{5d}] &= TPW1_{2,1} \cdot [p_{6a} + p_{6b} + p_{6c} + p_{6d}] \\ &+ TPW1_{2,2} \cdot \rho_o c_c [u_{6a} + u_{6b} + u_{6c} + u_{6d}] \end{aligned} \quad \text{(C6)}$$

where

$$p_5 = p_{5a} = p_{5b} = p_{5c} = p_{5d} ;$$

$$p_6 = p_{6a} = p_{6b} = p_{6c} = p_{6d} ;$$

$$u_5 = u_{5a} + u_{5b} + u_{5c} + u_{5d} ;$$

$$u_6 = u_{6a} + u_{6b} + u_{6c} + u_{6d} \quad \text{(C7)}$$

Plugging Eq. (C7) into Eqs. (C5) and (C6) yields

$$4 \cdot p_5 = 4 \cdot TPW1_{1,1} \cdot p_6 + TPW1_{1,2} \cdot \rho_o c_c u_6 \quad \text{(C8a)}$$

$$\rho_o c_o u_5 = 4 \cdot TPW1_{2,1} \cdot p_6 + TPW1_{2,2} \cdot \rho_o c_c u_6 \quad \text{(C8b)}$$

Rearranging Eq. (C8) in a matrix form, the equivalent four-pole matrix between nodes 5 and 6 shown in Fig. 4 is

$$\begin{bmatrix} p_5 \\ \rho_o c_o u_5 \end{bmatrix} = \begin{bmatrix} TPW1_{1,1} & \frac{1}{4} \cdot TPW1_{1,2} \\ 4 \cdot TPW1_{2,1} & TPW1_{2,2} \end{bmatrix} \begin{bmatrix} p_6 \\ \rho_o c_o u_6 \end{bmatrix} \quad \text{(C9)}$$

REFERENCES

Chang, Y. C., L. J. Yeh, M. C. Chiu and G. J. Lai (2005). Shape optimization on constrained single-layer sound absorber by using GA method and mathematical gradient methods. Journal of Sound and Vibration 1286(4-5), 941-961.

Chiu, M. C. (2010a). Shape optimisation of multi-chamber mufflers with plug-inlet tube on a venting process by genetic algorithms. Applied Acoustics 71, 495-505.

Chiu, M. C. (2010b). Optimal design of multi-chamber mufflers hybridized with perforated intruding inlets and resonated tube using simulated annealing. ASME J. of Vibration and Acoustics 132, 1-10.

Chiu, M. C. (2011a). Optimization design of hybrid mufflers on broadband frequencies using the genetic algorithm. Archives of Acoustics 36(4) 795-822.

Chiu, M. C. (2011b). Numerical assessment of hybrid mufflers on a venting system within a limited back pressure and space using simulated annealing. J. of Low Frequency Noise, Vibration and Active Control 30(4), 247-275.

Chiu, M. C. and Y. C. Chang (2011). Numerical assessment of a venting system with multi-chamber perforated mufflers by ga method. Journal of Marine Science and Technology 19(5), 483-498.

Chiu, M. C. (2012). Genetic algorithm optimization on a venting system with three-chamber hybrid mufflers within a constrained back pressure and space. ASME J. of Vibration and Acoustics 134, 021005, 1-11.

Cummings, A. and I. J. Chang (1988). Sound attenuation of a finite length dissipative flow duct silencer with internal mean flow in the absorbent. Journal of Sound and Vibration 127, 1-17.

Jayaraman, K. and K. Yam (1981). Decoupling approach to modeling perforated tube muffler component. Journal of the Acoustical Society of America 69(2), 390-396.

Kar, T. and M. L. Munjal (2005). Generalized analysis of a muffler with any number of interacting ducts. Journal of Sound and Vibration 285, 585-596.

Kirkpatrick, S., C. D. Gelatt and M. P. Vecchi (1983). Optimization by simulated annealing. Science 220, 671-680.

Ko, S. H. (1975). Theoretical analyses of sound attenuation in acoustically lined flow ducts separated by porous splitters (rectangular, annular and circular ducts), propagation of sound between walls of porous material. Journal of Sound and Vibration 39, 471-487.

Lee, I. J. (2005). Acoustic characteristics of perforated dissipative and hybrid silencers. Ph. D. Thesis, Ohio State University, USA.

Lee, L. and A. Selamet (2006). Impact of perforation impedance on the transmission loss of reactive and dissipative silencers. Journal of the Acoustical Society of America 120(6), 3706-3713.

Metropolis, A., W. Rosenbluth, M. N. Rosenbluth, H. Teller and E. Teller (1953). Equation of static calculations by fast computing machines. The

Journal of Chemical Physics 21, 1087-1092.
Morse, P. M.(1939). Transmission of sound Inside pipes. Journal of the Acoustical Society of America 11, 205-210.
Munjal, M. L., K. N. Rao and A. D. Sahasrabudhe (1987). Aeroacoustic analysis of perforated muffler components. Journal of Sound and Vibration 114(2), 173-188.
Munjal, M. L. (1987). Acoustics of Ducts and Mufflers with Application to Exhaust and Ventilation System Design. John Wiley & Sons, New York.
Peat, K. S. (1988). A numerical decoupling analysis of perforated pipe silencer elements. Journal of Sound and Vibration 123(2),199-212.
Peat, K. S. (1991). A transfer-matrix for an absorption silencer element. Journal of Sound and Vibration 146, 353-360.
Rao, K. N. and M. L. Munjal (1984). A generalized decoupling method for analyzing perforated element mufflers. Nelson Acoustics Conference.
Sathyanarayana, Y. and M. L. Munjal (2000). A hybrid approach for aeroacoustic analysis of the engine exhaust system. Applied Acoustics 60, 425-450.
Selamet, A., I. J. Lee, Z. L. Ji and N. T. Huff (2001). Acoustic attenuation performance of perforated concentric absorbing silencers. SAE Noise and Vibration Conference and Exposition 2001-01-1435.
Selamet, A., I. J. Lee and N. T. Huff (2003). Acoustic attenuation of hybrid silencers. Journal of Sound and Vibration 262, 509-527.
Sohei, N., N. Tsuyoshi and Y. Takashi (2006). Acoustic analysis of elliptical muffler chamber having a perforated pipe. Journal of Sound and Vibration 297, 761-73.
Sullivan, J. W. and M. J. Crocker (1978). Analysis of concentric tube resonators having unpartitioned Cavities. Journal of the Acoustical Society of America 64, 207-215.
Sullivan, J. W. (1979). A method of modeling perforated tube muffler components I: theory. Journal of the Acoustical Society of America 66, 772-778.
Thawani, P. T. and K. Jayaraman (1983). Modeling and applications of straight-through resonators. Journal of the Acoustical Society of America 73(4), 1387-1399.
Xu, M. L., A. Selamet, I. J. Lee and N. T. Huff (2004). Sound attenuation in dissipative expansion chambers. Journal of Sound and Vibration 272, 1125-1133.